Süleyman Demirel Üniversitesi
Fen Bilimleri Enstitüsü Dergisi
Cilt 28, Sayı 2, 281-292, 2024

Süleyman Demirel University
Journal of Natural and Applied Sciences
Volume 28, Issue 2, 281-292, 2024

DOI: 10.19113/sdufenbed.1474689

Aldose Reductase Evaluation against Diabetic Complications Using ADME and Molecular Docking Studies and DFT Calculations of Spiroindoline Derivative Molecule

Kenan GÖREN*[1], Ümit YILDIKO[2]

[1]Kafkas University, Faculty of Science and Arts, Department of Chemistry, Kars, Turkey
[2]Kafkas University, Architecture and Engineering Faculty, Department of Bioengeering, Kars, Turkey

(Alınış / Received: 27.04.2024, Kabul / Accepted: 13.08.2024, Online Yayınlanma / Published Online: 23.08.2024)

Keywords
Spiroindoline Derivative,
DFT,
Molecular Docking,
MEP,
ADME,
NBO

Abstract: In this study, the target molecule ethyl-2-(5-nitro-5'-(4-nitrophenyl)-2-oxo-3'H-spiro[indoline-3,2'-[1,3,4]oxadiazol]-1-yl)acetate, which is a spiroindoline derivative, were performed NBO analysis, molecular electrostatic potential surface (MEPS), nonlinear optics (NLO), HOMO-LUMO energy calculations, optimized molecular geometry, and mulliken atomic charges using B3LYP/B3PW91 basis set and 6-311G(d,p) approximations. Calculated results were reported. Density Functional Theory (DFT) computations were utilized to research the molecule theoretically. Moreover, molecular docking analysis of the tested compound, a spiroindoline derivative molecule targeting aldose reductase against diabetic complications, was performed using molecular docking to determine the structure-activity connection. The molecular docking scores of our study molecule showed good results of -6.83 (PDB ID:3ABV) and 6.78 (PDB ID:3AE2) kcal. The molecular docking study provided important information worth considering for further research. A notable outcome of bioisosteric and isosteric substitutions is the alteration in lipophilic character, an impressive characteristic in several aspects. Thus, utilizing SwissADME, lipophilic character assessments were performed for the concerned compounds.

Spiroindolin Türevi Molekülünün DFT Hesaplamaları ve ADME ve Moleküler Doking Çalışmaları Kullanılarak Diyabetik Komplikasyonlara Karşı Aldoz Redüktaz Değerlendirmesi

Anahtar Kelimeler
Spiroindolin Türevi,
DFT,
Molecular Doking,
MEP,
ADME,
NBO

Özet: Bu çalışmada, spiroindolin türevi olan, hedef molekül etil-2-(5-nitro-5'-(4-nitrofenil)-2-okso-3'H-spiro[indolin-3,2'-[1,3,4]oksadiazol]-1-il)asetat'in B3PW91/B3LYP temel set ve 6-311G(d,p) yaklaşımlar kullanılarak NBO analizi, moleküler elektrostatik potansiyel yüzey (MEPS), HOMO-LUMO enerji hesaplamaları, doğrusal olmayan optik (NLO), optimize edilmiş moleküler geometri ve mulliken atomik yükleri hesaplamaları yapıldı. Hesaplanan sonuçlar açıklandı. Molekülün teorik olarak incelenmesi için Yoğunluk Fonksiyonel Teorisi (DFT) hesaplamaları kullanıldı. Ayrıca, diyabet komplikasyonlarına karşı aldoz redüktazı hedef alan spiroindolin türevi molekülü olan test edilen bileşiğin yapı-aktivite bağlantısını belirlemek amacıyla moleküler doking analizi yapıldı. Çalışma molekülümüzün moleküler doking skorları -6,83 (PDB ID:3ABV) ve 6,78 (PDB ID:3AE2) kcal gibi iyi sonuçlar verdi. Moleküler doking çalışması, ileri araştırmalar için dikkate değer önemli bilgiler sağladı. Biyoizosterik ve izosterik yer değiştirmelerin dikkate değer bir sonucu, çeşitli yönlerden etkileyici bir özellik olan lipofilik karakterdeki değişikliktir. Bu yüzden SwissADME kullanılarak söz konusu bileşikler için lipofilik karakter değerlendirmeleri yapılmıştır.

1. Introduction

During a hyperglycemic condition, aldose reductase, a NADPH-dependent oxidoreductase, is crucial for the catalytic synthesis of sorbitol from glucose. Such enzyme is a crucial part of the polyol the route that is the body's natural means of breaking down a little amount of unphosphorylated glucose [1]. The enzyme sorbitol dehydrogenase then helps sorbitol be converted to fructose. It is noteworthy that a major

*Corresponding author: kenangoren49@gmail.com

factor in cell and organ damage is osmotic stress, which is linked to sorbitol buildup and redox imbalance after NADPH depletion [2]. As a result, cataracts, neuropathy, retinopathy, nephropathy, and other diabetes problems eventually develop. Congestive heart failure, myocardial is chemia, and cardiac arrest are among the cardiovascular disorders that are eventually brought on by this. Reactive oxygen species produced by elevated AR are also thought to be the cause of many cancers, including those of the breast, liver, cervix, ovarian, and rectal regions [3]. Acknowledging AR inhibition as a critical tactic to avoid and mitigate long-term diabetes consequences has gained significance [4, 5]. Therefore, we carried out molecular docking research in an effort to find efficient therapies for diabetes complications.

One excellent example of a diverse collection of chemical compounds formed from isatin is spirogynole. These substances are rich in physiologically relevant natural products with multifunctional pharmacological activity and have extraordinary biological features. They also make up a large portion of medications [6]. The presence of many heterocyclic motifs that attach to the oxindole ring's C-3 position is the distinguishing characteristic of spirooxindoles. They are promising candidates for drug development because of their special position [7]. Synergistic effects are frequently observed when bioactive macromolecules with various ranges of action or complementing pharmacophoric components are used together. Thus, an important endeavor to stop the drug is still being done in persistently advanced investigations [8].

Information regarding the pharmacological characteristics of molecular systems may be obtained by theoretical methods like molecular docking and DFT. DFT is a technique used in many-body systems to approximate the solution of the Schrödinger equation [9]. Walter Kohn chose the electron density, a function of both space and time, as a fundamental variable in a 1964 research he did with P. Hohenberg. He said that using the many-body wave function as a fundamental variable in a variational approximation complicated the issue [10].

The structure of the molecule studied theoretically was taken from the literatüre [11]. The optimal structural characteristics, stabilization energy, and chemical bonding of the molecule derived from spiroindoline are presented in this work. The band gap energies were computed using molecular orbitals. The parameters of ADME and drug similarity were examined. The molecule, a derivative of spiroindoline, was predicted theoretically utilizing the DFT technique, the B3LYP/B3PW91 basis set and 6-311G(d,p) approximations. Furthermore, our drug underwent molecular docking investigations, and binding energies and interaction types were computed for the spiroindoline derivative molecule targeting aldose reductase against diabetes sequelae.

2. Material and Method

All of the study's quantum chemical computations were carried with the Gaussian 09 software, B3LYP/6-311G(d,p)-B3PW91/6-311G(d,p) basis sets and approximations, and DFT methodologies [12]. Data on molecules were plotted and shown in GaussView 6.0. Our molecule's various charges were compared in the graph using the Origin 2019b 64Bit application. Our compound was subjected to a molecular docking investigation utilizing the Schrödinger LLC model on the Maestro Molecular Modeling platform (version 12.5) [13]. The enzyme for our molecule was obtained from the Protein Data Bank (PDB ID:3ABV and 3AE2) in order to conduct molecular docking investigations [14]. Using the Discovery Studio 2021 Client application, molecular docking pictures of our compound were obtained [15]. Lastly, the ADME analysis in our study was conducted using the online database SwissADME [16].

3. Results

3.1. Structure details and analysis

The most stable and lowest energy state of a molecule is known as geometry optimization [17]. Gaussian 09W software was employed in the investigation to finalize the spiroindoline derivative molecule's optimal shape [12]. Calculated results for some structural characteristics (bond angles, bond lengths) optimized using B3LYP/B3PW91 basis set and 6-311G(d,p) approximations for quantum chemical calculations with DFT approach Table 1 It is listed in. One variational approach is DFT. The BLYP (Becke, Lee, Yang, and Parr) technique and the B3LYP technique, which was developed by modifying BLYP, are the most often used DFT methods. In very large nuclei, electrons close to the nucleus are considered approximately effective nuclear potentials (ECPs). Relativistic effects play a significant role in this behavior for these atoms [18]. The spiroindoline derivative molecule was examined by comparing two optimized base sets. We observed that there were very small differences in bond lengths and angles between the basis sets and approaches used. The aromatic ring's optimal bond lengths and bond angles are between typical ranges. It has been found that our molecule's the C-C aromatic bond distances had higher values in the B3LYP computation compared to the B3PW91 method. The bond lengths optimized of C–C in the aromatic benzene fall in the range of 1.443 to 1.512 Å for the B3LYP/6-311G(d,p) technique and

in the range of 1.439 to 1.507 Å to the B3PW91/6-311G(d,p). The elongation due to displacements make the bond lengths evident. In the ring, C23-H46 and C5-H38 bond lengths are longer than other C-H bonds because of the substitution of oxygen and nitrogen atoms. Methyl C-H bond lengths have the same impact. It was discovered that the bond angle between C25-C24-N30-O31 in tetrahedral structures had the largest deviation at -179.67798°. C8-C7-N11-N12 The lowest change in bond angle is -156.57642°. We saw that when atoms were selected as dihedral bonds in the Gaussian 09 program, some dihedral angles gave negative results in angle degrees, while others gave positive values.

Table 1. The spiroindoline derivative molecule's theoretically determined some bond lengths (Å) and bond angles (°)

Bond Lengths	B3PW91/ 6-311G(d,p)	B3LYP/ 6-311G(d,p)	Bond Lengths	B3PW91/ 6-311G(d,p)	B3LYP/ 6-311G(d,p)
C1-N27	1.38806	1.39374	**C7-O10**	2.76229	2.78096
C3-C7	1.43965	1.44370	**N12-C13**	1.36783	1.37165
C4-N9	1.45544	1.46109	**C13-C14**	1.48921	1.49376
C8-O15	1.20977	1.20896	**C13-O10**	1.23470	1.23652
N9-C16	1.48397	1.49069	**C24-N30**	1.38214	1.38750
C17-O18	1.19713	1.19850	**N30-O31**	1.24010	1.24602
O19-C20	1.45150	1.45973	**N30-O32**	1.39726	1.41029
C20-C21	1.50786	1.51264	**C16-H33**	1.08848	1.08769
C7-N11	1.38020	1.38754	**N11-H39**	1.01234	1.01263
N11-N12	1.32799	1.33500	**C23-H46**	1.08235	1.08122
Bond Angles	**B3PW91/ 6-311G(d,p)**	**B3LYP/ 6-311G(d,p)**	**Bond Angles**	**B3PW91/ 6-311G(d,p)**	**B3LYP/ 6-311G(d,p)**
O28-N27-O29	118.23984	118.13535	**C3 -C7-O10**	111.84539	112.32317
C1-N27-O29	115.08418	115.07689	**N9-C8-O15**	117.49646	117.24558
C2-N27-C1	120.53120	120.49629	**C16-C17-O19**	117.49646	110.60899
C2-C3-C7	131.89445	131.56935	**N12-C13-O10**	110.56337	125.85262
C4-C5-N9	126.66730	126.62472	**C24-N30-O31**	127.26668	127.37411
Planar Bond Angles	**B3PW91/ 6-311G(d,p)**	**B3LYP/ 6-311G(d,p)**	**Planar Bond Angles**	**B3PW91/ 6-311G(d,p)**	**B3LYP/ 6-311G(d,p)**
C6-C1-N27-O29	-178.37363	-178.38623	**C8-C7-N11-N12**	-156.57642	-154.86457
C16-C17-O19-C20	-177.16420	-176.19686	**O10-C13-C14-C26**	177.86945	177.73634
C4-N9-C16-C17	-165.90029	-167.85701	**C23-C24-N30-O32**	-179.63563	-179.65346
C5-C1-N27-O29	-178.37363	-178.38623	**C25-C24-N30-O31**	-179.67798	-179.73446

3.2. Mulliken atomic charges

Charge of an atom has been utilized to determine the electrostatic potential outside molecule surfaces and to analyze electronegativity equalization and charge transfer in processes [19]. Mulliken atomic charges are crucial for describing the electronic charge distribution within a molecule as they are based on the atoms' the electronic charges that make up the molecule [20]. Table 2 displays the mulliken atomic charges that were determined utilizing the B3LYP/B3PW91 basis set and 6-311G(d,p) approximations estimates to the molecule corresponding to the spiroindoline derivative. The electron density is redistributed at atoms C14, C25, C22, O10, N12, and N30 when the aromatic ring has negative values. The C7 and C13 carbon atoms have positive charges because of the significant negative charges on the nitrogen atoms N11 and N12. It was noted that the C atoms were both positive and negative.

Furthermore, Figure 2 provides a) Structure Optimization, b) Bond Lengths, c) Atomic Mass, and d) Mulliken Charges utilizing the B3PW91/6-311G(d,p) basis set and method. The graph in Figure 1 compares the mulliken charges of a few C atoms in our molecule using the same basis sets and methods. We found that the basis sets and methods employed in this comparison had mulliken loads that are compatible with one another.

Table 2. Mulliken Atomic Charges of the spiroindoline derivative molecule

ATOMS	B3PW91/ 6-311G(d,p)	B3LYP/ 6-311G(d,p)	ATOMS	B3PW91/ 6-311G(d,p)	B3LYP/ 6-311G(d,p)
C2	-0.023	-0.023	**N9**	-0.549	-0.513
C4	0.145	0.133	**O10**	-0.397	-0.391
C5	-0.049	-0.045	**N11**	-0.314	-0.289
C6	-0.109	-0.098	**N12**	-0.297	-0.277
C7	0.166	0.161	**N27**	-0.006	-0.010
C8	0.314	0.287	**O28**	-0.329	-0.319

C13	0.364	0.334	**O29**	0.256	0.254
C14	-0.216	-0.210	**N30**	-0.003	-0.013
C16	-0.126	-0.103	**O31**	-0.338	-0.328
C17	0.396	0.379	**O32**	-0.269	-0.270
C20	-0.057	0.023	**H33**	0.203	0.182
C21	-0.357	-0.314	**H34**	0.191	0.173
C22	-0.045	0.040	**H36**	0.160	0.141
C23	-0.099	-0.090	**H38**	0.141	0.128
C25	-0.109	-0.100	**H40**	0.150	0.145
C40	-0.035	-0.031	**H42**	0.139	0.121

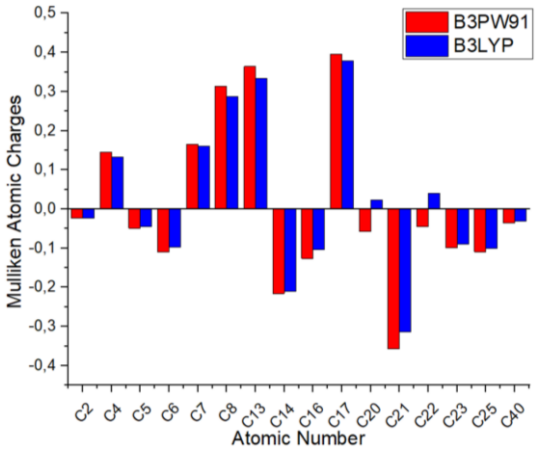

Figure 1. Mulliken atomic charge comparison for the spiroindoline derivative molecule

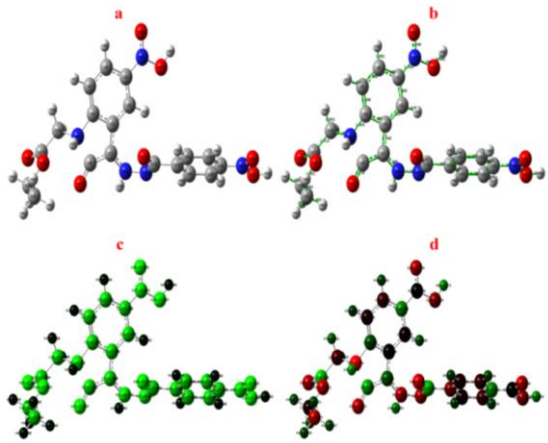

Figure 2. The spiroindoline derivative molecule with DFT/B3PW91/6-311G(d,p) basis set a) Structure Optimization, b) Bond Lengths, c) Atomic Mass, d) Mulliken Charge

3.3. HOMO and LUMO analysis

The reactivity, bioactivity, and electrical characteristics of organic molecules are explained in part by the FMO hypothesis. HOMO energy is a representation of electron donation. In reactivity analysis, it is crucial to estimate the energy values of

a given molecule's HOMO and LUMO, as well as to ascertain its locations [21]. Utilizing the energy gap (ΔE) that is determined by subtracting the LUMO and HOMO energies, together with many significant quantum chemical characteristics, is a very efficient method in computational chemistry for predicting the reactivity of a given molecule. Values for HOMO-LUMO energy are taken straight out the Gaussian output files [22]. Table 3 displays quantum chemical reactivity descriptors computed with these energy values. From the HOMO-LUMO energy values, the global chemical reactivity descriptors of our molecule like electronegativity (χ), global hardness (η), global softness (S) and electrophilicity index (ω) are 1.6464 to the B3PW91/6-311G(d,p) basis set and approach, respectively, 1.2080, 0.6040 and -5.0958. These calculations are χ=1.4590, η=1.2144, S=0.6072, and ω=5.0612 for the B3LYP/6-311G(d,p) basis set and approximation. As given in Table 3, the energy difference values for the two base and set approaches were calculated as 2.4360 eV and 2.4288 eV, respectively. Figure 3 and Figure 4 show 3D HOMO-LUMO diagrams with energy values in line with computed utilizing B3LYP/6-311G(d,p)-B3PW91/6-311G(d,p) basis sets and approximations. For both methods, it is clear that HOMOs are distributed almost throughout the molecule. Figure 5 and Figure 6 show the Fermi energy (Ef) and band gap of our working molecule using the same two basis set approaches.

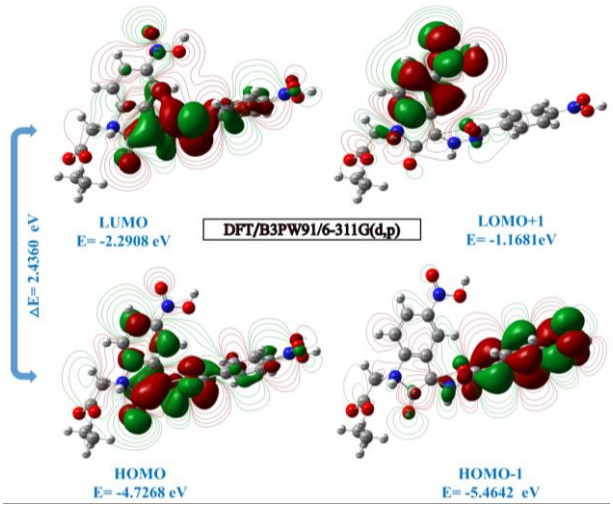

Figure 3. The spiroindoline derivative molecule's boundary molecular orbitals as per the B3PW91/6-311G(d,p) level

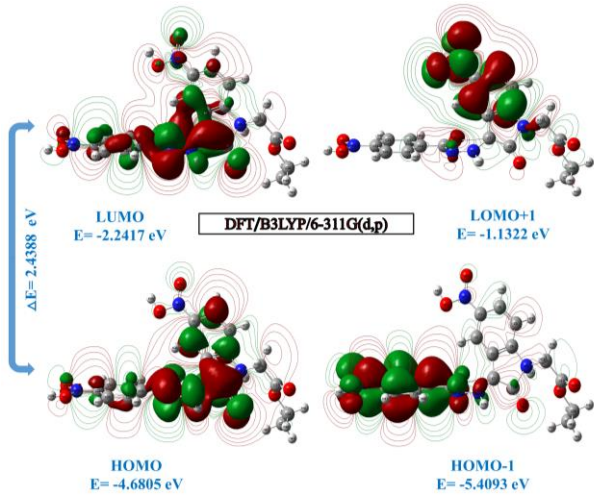

Figure 4. The spiroindoline derivative molecule's boundary molecular orbitals as per the B3LYP/6-311G(d,p) level

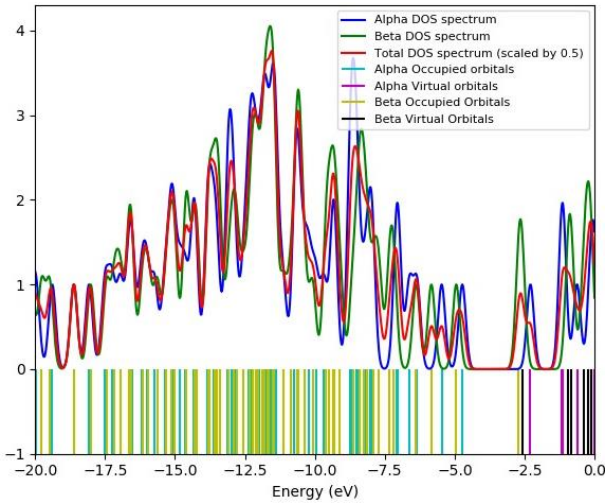

Figure 5. Fermi energy (Ef) and bandgap of the spiroindoline derivative molecule with B3PW91/6-311G(d,p) basis set

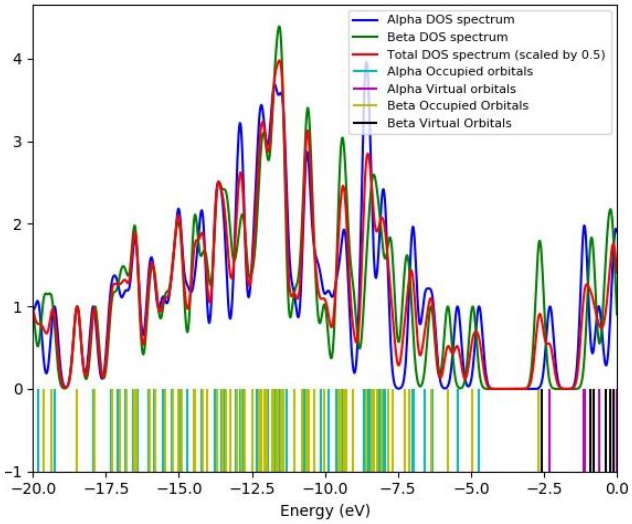

Figure 6. Fermi energy (Ef) and bandgap of the spiroindoline derivative molecule with B3LYP/6-311G(d,p) basis set

Table 3. Spiroindoline derivative molecule's computed quantum chemical properties by B3PW91/B3LYP/6-311G(d,p) techniques

Molecules Energy		**DFT/B3PW91/ 6-311G(d,p)**	**DFT/B3LYP/ 6-311G(d,p)**
E_{LUMO}		-2.2908	-2.2417
E_{HOMO}		-4.7268	-4.6805
E_{LUMO+1}		-1.1681	-1.1322
E_{HOMO-1}		-5.4642	-5.4093
Energy Gap	$(\Delta E)\lvert E_{HOMO}-E_{LUMO}/$	2.4360	2.4388
Ionization Potential	$(I=-E_{HOMO})$	4.7268	4.6805
Electron Affinity	$(A=-E_{LUMO})$	2.2908	2.2417
Chemical hardness	$(\eta=(I-A)/2)$	1.2080	1.2194
Chemical softness	$(s=1/2\eta)$	0.6040	0.6097
Chemical Potential	$(\mu=-(I+A)/2)$	-3.5088	-3.5596
Electronegativity	$(\chi=(1+A)/2)$	1.6464	1.6208
Electrophilicity index	$(\omega=\mu^2/2\eta)$	5.0958	5.1954

3.4. Molecular electrostatic potential (MEP)

The use of MEP surface analysis yields limitations for forecasting the electrophilic and nucleophilic assaults of any chemical compound and offers information about the chemical reactivity of a molecule. One instrument that gives information on the size, shape, and the molecule's electrostatic potential values is the commonly used MEP [23]. Furthermore, the names of biological processes and the demonstration of hydrogen bond interactions in molecular modeling studies are attributed to the reactive moieties in chemical reactions. Different hues correspond to different electrostatic potential levels on the surface. The potentials are arranged as follows: red<orange<yellow<green<blue [24]. Figure 7. shows the MEP surface obtained following the computation with B3LYP/B3PW91 basis set and 6-311G(d,p)

approximations. The electronegative O atom has negative potential areas, shown in Figure 7. The positive potential represented in blue was obtained in the C–H and N–H bond areas. Electrophilic areas on the surface of the oxygen and nitrogen groups in our molecule show that red-colored areas represent negative prospective areas.

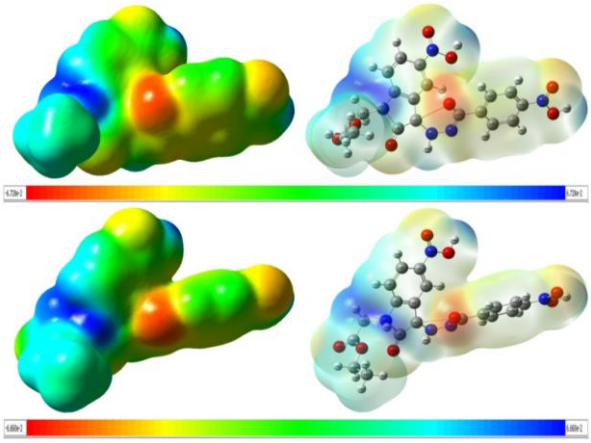

Figure 7. MEP of the spiroindoline derivative molecule utilizing DFT(B3PW91/B3LYP) and 6-311G(d,p) approximation and basis sets

3.5. Non-Linear Optical Properties (NLO)

Electromagnetic beam interaction in a variety of situations can produce new fields with different phase, frequency, amplitude, and other propagation properties than the incident fields. This phenomenon is known as NLO results [25]. NLO is at the forefront of current research due to its critical role in providing Because of its vital role in providing functionalities like optical modulation, frequency shifting, optical switching, optical logic, and optical memory for developing technologies in fields like telecommunications, optical interconnects, and signal processing, NLO is at the forefront of current research [26]. Our study molecule's polar features of were calculated with the DFT B3LYP/B3PW91 basis set and 6-311G(d,p) approximations utilizing the Gaussian 09W package. In this investigation, we effectively investigated DFT-NLO materials by calculating linear polarizability (α), the total molecular dipole moment (μ), and first-order hyperpolarizability (β) from the gaussian. These results are listed in Table 4. Equations (1) through (3) may be used since the values of the initial hyperpolarization tensors of the Gaussian 09W output file are given in atomic units (a.u.), the computed values are transformed to electrostatic units (1 a.u.=8.6393×10^{-33} esu) for both methods. It was found to be 2.48x10^{-30} and 2.56x10^{-30} esu, respectively. The predominance of one component over another suggests a large movement of loads in that direction. The highest hyperpolarizability values were found in the βYYY direction, which was also where the electron cloud's delocalization was greatest. The urea molecule is one of the model molecules used in studies on systems that exhibit NLO properties. The computed values of μ and β for both approaches are around four and seven times, respectively, more than those of the typical NLO material "urea." The relatively large dipole moment and hyperpolarizability of our compound may indicate that The substance can serve as a foundational element for NLO materials.

$$\mu = (\mu_x^2 + \mu_z^2)^{1/2} \quad (1)$$

$$\beta_{Total} = (\beta^2 x + \beta^2 y + \beta^2 z)^{1/2} \quad (2)$$

$$\beta_{Total} = [(\beta xxx + \beta xyy + \beta xzz)^2 + (\beta yyy + \beta yxx + yzz)^2 + (\beta zzz + \beta zxx + \beta zyy)^2]^{\frac{1}{2}} \quad (3)$$

Table 4. The spiroindoline derivative molecule's NLO parameters computed utilizing B3PW91/B3LYP and 6-311G(d,p) approaches and basis set

Parameters	B3PW91/ 6-311G(d,p)	B3LYP/ 6-311G(d,p)	Parameters	B3PW91/ 6-311G(d,p)	B3LYP/ 6-311G(d,p)
μ_x	-6.0785	6.1785	β_{XXX}	-5.7848	18.5127
μ_y	1.6220	1.4563	β_{YYY}	-43.9294	-49.2287
μ_z	0.2028	-0.1940	β_{ZZZ}	-1.3001	2.3678
$\mu_{(D)}$	6.2944	6.3507	β_{XYY}	-13.003	13.4038
αXX	-152.8694	-156.4866	β_{XXY}	-5.0991	-5.1296
α_{YY}	-184.3685	-185.6480	β_{XXZ}	43.2432	-41.8450
αZZ	-182.6224	-184.0751	β_{XZZ}	-14.6662	13.3821
α_{XY}	-0.1931	0.1666	β_{YZZ}	-6.2615	-5.1861
α_{XZ}	-29.1015	-28.7701	β_{YYZ}	-0.1764	0.4113
α_{YZ}	-3.7211	3.9983	β_{XYZ}	41.9318	41.2029
α(au)	-165.168	-163.827	β(esu)	2.48x10^{-30}	2.56x10^{-30}

3.6. NBO analysis

The most precise "natural Lewis structure" image is produced by NBO analysis because every orbital feature is mathematically selected to have the maximum percentage of electron density. The NBO

method's ability to offer details on interactions in both virtual and occupied orbital spaces is a helpful feature that can improve the investigation of intra- and intermolecular mutual effect [27]. The interactions lead to an empty non-Lewis orbital and the loss of occupancy of the localized NBO of the ideal Lewis structure. For each donor (i) and acceptor (j), the stabilization energy E(2) associated with delocalization i→j is given by where qi is the donor orbital occupancy, εj and εi are diagonal elements, and F(i, j) is predicted [28]. Natural bond analysis is used to understand distinct secondary interactions between occupied orbitals of one subsystem and unoccupied orbitals of another subsystem, which is known as intermolecular delocalization. The fact that NBO analysis offers details on both occupied and vacant orbital spaces is a helpful feature that can improve the examination of intra- and extramolecular effects [29]. The NBO analysis of the spiroindoline derivative molecule was computed with the B3LYP/6-311G(d,p) basis set and approache to explain the delocalization and hybridization of the molecule's the electron density, and the NBO analysis values are in Table 5. is also given. When Table 5 is examined, the existence of strong interactions and charge transitions within the molecule is clearly observed. According to the results calculated with the DFT(B3LYP/6-311G(d,p) basis set approach, the highest energy value is 15.41 kcal/mol between π(C23-C24)→π*(C14-C22). The other highest energy values obtained are (C3-C4)→π*(C5-C6) 15.04 kcal/mol, (C1-C2)→π*(C3-C4) 15.02 kcal/mol, (C14-C22)→π*(C25-C26) 14.24 kcal/mol, (C7-N11)→π*(C8-O15) 13.87kcal/mol, (C25-C26)→π*(C23-C24) 12.86 kcal/mol.

Table 5. Chosen NBO outcomes of the spiroindoline derivative molecule are computed utilizing DFT(B3LYP/6-311G(d,p) technique and basis set

NBO(i)	Type	Occupancies	NBO(j)	Type	Occupancies	E(2)[a] (Kcal/mol)	E (j)-E(i)[b] (a.u.)	F (i, j)[c] (a.u)
C1-C2	π	0.81618	**C3-C4**	π*	0.82900	15.02	0.28	0.084
C3-C4	π	0.82900	**C5-C6**	π*	0.86892	15.04	0.29	0.083
C4-N9	σ	0.99160	**C5-C6**	σ*	0.86892	5.17	1.37	0.053
C5-C6	π	0.86892	**C1-C2**	π*	0.81618	11.55	0.28	0.076
C7-C8	σ	0.98506	**C3-C7**	σ*	0.98073	5.52	0.28	0.076
C7-N11	π	0.85730	**C8-O15**	π*	0.99736	13.87	0.32	0.084
C8-O15	σ	0.99736	**C7-C8**	σ*	0.98506	2.10	1.64	0.075
N11-H39	σ	0.98898	**C3-C7**	σ*	0.98073	2.33	1.15	0.065
C14-C22	π	0.81044	**C25-C26**	π*	0.86874	14.24	0.28	0.081
C14-C26	σ	0.98732	**C14-C22**	σ*	0.81044	2.05	1.25	0.064
C16-C17	σ	0.98709	**O19-C20**	σ*	0.99318	2.20	0.91	0.057
C16-H34	σ	0.98361	**C17-O18**	π*	0.99502	2.54	0.58	0.051
C21-H42	σ	0.98993	**019-C20**	σ*	0.99318	2.29	0.74	0.052
C22-H45	σ	0.98833	**C14-C26**	σ*	0.98732	2.31	1.07	0.063
C23-C24	π	0.80307	**C14-C22**	π*	0.81044	15.41	0.29	0.08
C23-H46	σ	0.98880	**C24-C25**	σ*	0.98543	2.20	1.06	0.061
C24-C25	σ	0.98543	**C23-C24**	σ*	0.98338	2.50	1.24	0.070
C24-N30	σ	0.99436	**C24-C25**	σ*	0.98543	5.34	1.41	0.045
C25-C26	π	0.86874	**C23-C24**	π*	0.80307	12.86	0.27	0.079
C25-H47	σ	0.98859	**C23-C24**	σ*	0.98338	2.15	1.06	0.060
C26-H48	σ	0.98816	**C24-C25**	σ*	0.98543	2.19	1.04	0.060
N27-O28	σ	0.99678	**C1-N27**	σ*	0.99397	5.19	1.44	0.045
N27-O29	σ	0.99570	**C1-C6**	σ*	0.98377	3.33	1.41	0.046
O29-H49	σ	0.99440	**C1-N27**	σ*	0.99397	1.88	1.16	0.060
N30-O31	σ	0.99681	**C24-C25**	σ*	0.98543	0.56	1.59	0.038
O32-H50	σ	0.99467	**C24-N30**	σ*	0.99436	1.81	1.17	0.059

3.7. Molecular docking studies

A key component of medication design for the treatment of numerous disorders is molecular docking. During this procedure, we learned that a chemical may function as a medicine by attaching to a protein; for this reason, docking is crucial in the drug development process [30]. In molecular docking analysis, the enzyme for our molecule was taken from the Protein Data Bank (PDB ID: 3ABV and PDB ID: 3AE2) [14] and made with Schrödinger's Protein Preparation Wizard modüle [13]. This approach involved adding missing hydrogens, assigning bond ordering, and deleting all heteroatoms and water molecules other than the native ligand. The LigPrep module was used to prepare the ligand for all potential 3D conformations and states at physiological pH levels prior to molecular docking. The molecular docking scores of our study molecule gave good results as -6.83 (PDB ID:3ABV) and 6.78

(PDB ID:3AE2) kcal, and these values are given in Table 6. For molecular docking analysis, the best docking poses were selected and the protein-ligand interaction was shown visually in 2D-3D with Discovery Studio Client 2017 software in Figure 8 and Figure 9 [15].

The docking poses of our working molecule (PDB-CODE:3ABV) with the enzyme. The 2D and 3D docking poses we obtained from the Discovery Studio visualizer [15] are shown in Figure 8. When we analyze the molecule and ligand interaction, the best bindings are as follows; While we observe ARG-46 (3.12 Å) Unfavorable Donor-Donor, SER-53 (4.00 Å) and SER-42 (4.03 Å) conventional hydrogen bonds, GLY-49 (5.27 Å) pi-alkyl bond in the oxygen of the nitro group, We observed HIS-216 (4.77 Å) and HIS-45 (6.41 Å) pi-pi t-shaped bond, ARG-44 (5.87 Å) pi-cation bonds in the benzene ring. We observed İLE-218, İLE-218, İLE-84, TRP-82, LEU-52, VAL-87 and ARG-47 van der Waals bonds in our molecule.

Table 6. Docking score of the spiroindoline derivative molecule PDB:3ABV and PDB:3AE2

Compound	Docking Score (cal/mol)			
	PDB: 3ABV	Control 3ABV	PDB: 3AE2	Control 3AE2
The Spiroindoline Derivative Molecule	-6.83	-8.20	-6.78	-7.80

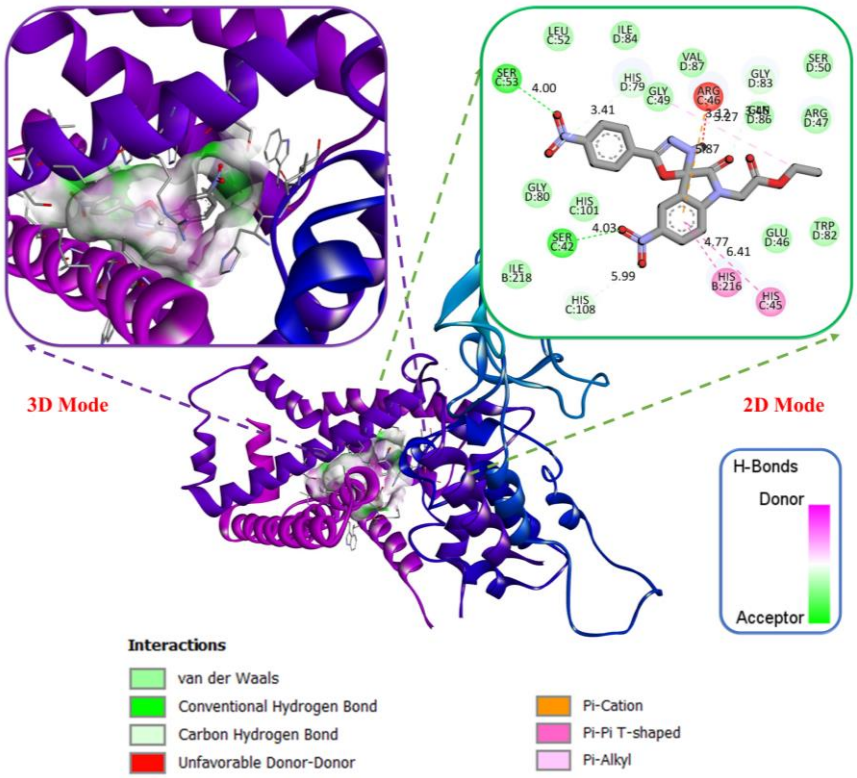

Figure 8. 3D and 2D representation of the interaction between the spiroindoline derivative molecule of 3ABV enzym

The docking poses of our study molecule (PDB-CODE:3AE2) with other enzymes. The 2D and 3D docking poses we obtained from the Discovery Studio visualizer are shown in Figure 9. When we analyze the molecule and ligand interaction, the best bindings are as follows; While we observed (5.26 Å) pi-alkyl bond TYR-91 (4.45 Å) pi-anion, ARG-46 (5.04 Å) attractice charge, HOH-1202 (3.07 Å) water hydrogen bond, TRP-172 (6.27 Å) pi-alkyl bond, MET-39 in the oxygen of the nitro group, we observed TYR-91 (4.05 Å) pi-cation bond and ARG-46 (4.58 Å) unfavorable positive-positive bond at the nitrogen of the nitro group. We observed TRP-173 (5.86 Å) pi-pi t-shaped bond, SER-42 (7.01 Å) amide-pi stacked bond, İLE-43 (4.22 Å), PRO-169 (5.69 Å) pi-alkyl bonds in the benzene ring. We observed HİS-216, İLE-218, İLE-30, ASN-220, TRP-35, and TYR-33 van der Waals bonds in our molecule.

According to our literature research, docking analysis was not performed on the protein structures we selected, so docking analysis was performed to compare the ethyl2-(5-nitro-2-oxo-5'-(pyridin-4-yl)-3'H-spiro[indoline-3,2'-[1,3,4]oxadiazol]-1-yl)acetate [11] (control ligand) structure, which has a similar structure to our molecule, with the same proteins. Figure 10. Control Ligand-3ABV 2D Mode and control Ligand-3AE2 2D Mode view shown. When we look at the docking scores in Table 6, it was seen that the binding scores of both proteins were close to the control ligand binding scores.

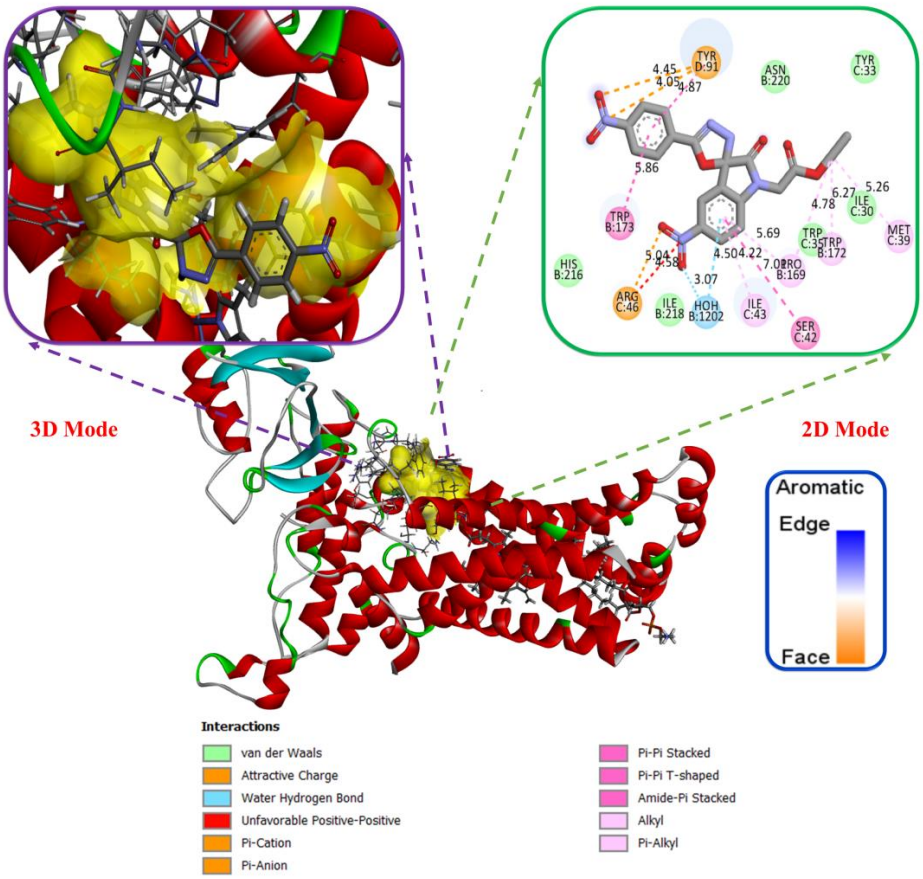

Figure 9. 3D and 2D representation of the interaction between the spiroindoline derivative molecule of 3AE2 enzym

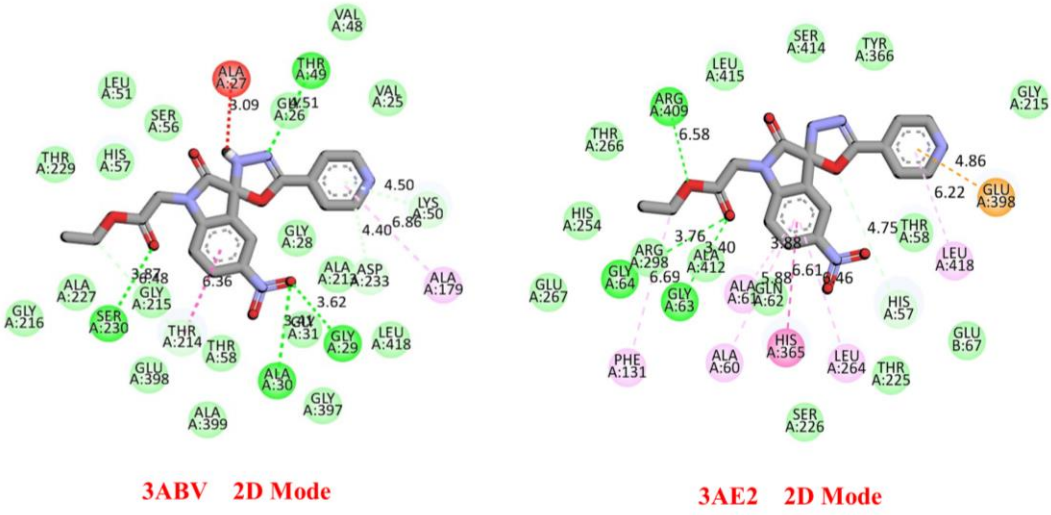

Figure 10. Control Ligand-3ABV and **control** Ligand-3AE2 2D Mode view

3.8. ADME analysis

ADME analysis is a useful tool in the drug development process for producing active pharmaceuticals. Examining the physicochemical characteristics is crucial for drug analysis. Lipophilicity is one of the most significant physicochemical characteristics. In pharmacology and the pharmaceutical business, estimates of the n-octanol/water partition coefficient (logPow) are significant because they enable assessments of lipophilic natüre [31]. For this purpose, SwissADME and its software were used [16]. This online application is likewise user-friendly and freely available. The physicochemical and lipophilic characteristics of our research substance are quantified numerically in Table 7. When we examine the values in Table 7, according to Lipinski's five

important rules; having less than 5 hydrogen bond donors (1), less than 10 hydrogen bond acceptors (9), lipophilicity coefficient LogP being less than 5 (0.94), molar refraction values between 4-130 (121.86) and finally We found that the molecular weight (MW) being lower than 500 (441.35) fits. It demonstrates that Lipinski's criteria has not been broken and that this molecule is appropriate for the drug development process. SwissADME software is used to account for the XLOGP3, iLOGP, MLOGP, SILICOS-IT, and WLOGP prediction models in the lipophilic character analysis. All models' arithmetic means are displayed as consensus logPow [32]. As shown in Table 7, the consensus logPow value for our molecule was computed to be 0.94. In Adme analysis, the absorption percent of our study molecule ABS was found to be 49.70%. The physicochemical properties, color spaces, and structure of our study molecule are shown in Figure 10. The pink region on polar surface area maps symbolizes the physicochemical area suitable for oral bioavailability. According to the radar diagram, it is aside from the saturation setting, in the pink region.

Table 7. Physicochemical and lipophilicity of the spiroindoline derivative molecule

Code Spiroindoline Derivative Molecule	**Lipophilicity consensus log P**	**Physico-chemical properties**								
		MW[a] g/mol	**Heavy Atoms**	**Aromatic heavy atoms**	**Rot. bond**	**H-acceptor bond**	**H-donor bond**	**MR[b]**	**TPSA[c] (A²)**	**% ABS[d]**
	0.94	441.35	32	12	7	9	1	121.86	171.87	49.70

[a]**MW**, molecular weight; [c]**TPSA**, topological polar surface area; [b]**MR**, molar refractivity; [d]**ABS%:** absorption percent $ABS\% = 109 - [0.345 \times TPSA]$.

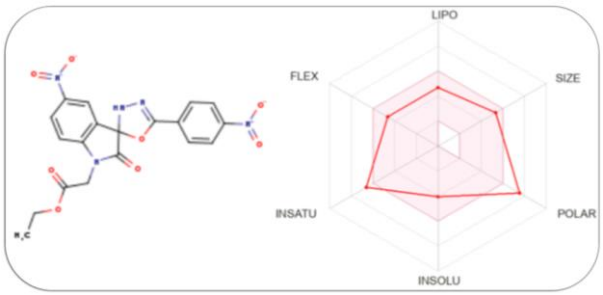

Figure 10. Color regions, physicochemical parameters and structure of the spiroindoline derivative molecule

4. Discussion and Conclusion

In this study, the spiroindoline derivative molecule was determined by optimizing the structure using DFT tools. We investigated the structural properties of [oxadiazol]-1-yl)acetate. In continuation of the theoretical calculations, mulliken charges, HOMO-LUMO, MEP, NLO, NBO analyzes of our study molecule were performed utilizing B3LYP/B3PW91 basis set and 6-311G(d,p) approximations. Polarity (α=-165.168 au and α=-163.827 au) and static higher order polarity ($2.48x10^{-30}$ esu and β=$2.56x10^{-30}$ esu) parameters were determined in the NLO analysis from the calculations made for the study molecule using two basis sets of approaches. In the HOMO-LUMO analysis, the basis sets and approaches used were calculated in harmony with each other as the difference in their energies (2.43 eV and 2.42). In the next stage of our study, molecular docking analysis of the spiroindoline derivative molecule focusing on aldose reductase to prevent problems from diabetes was performed by taking codes from the protein data bank (PDB ID: 3ABV and PDB ID: 3AE2). The two basis sets and approaches used gave good results as a result of molecular docking of -6.83 and -6.78 kcal/mol. Finally, in our study, ADME analysis of the molecule was performed. There is no corruption of Lipinski's rule of five in drug similarity predictions, and all rules apply to the title compound with respect to its drug nature. Molecular docking results confirm this result with binding energy. Therefore, we predict that our study molecule may be a potential drug candidate for Diabetic complications.

Declaration of Ethical Code

In this study, we undertake that all the rules required to be followed within the scope of the "Higher Education Institutions Scientific Research and Publication Ethics Directive" are complied with, and that none of the actions stated under the heading "Actions Against Scientific Research and Publication Ethics" are not carried out.

References

[1] Thakur, S., Gupta, S. K., Ali, V., Singh, P., Verma, M. 2021. Aldose Reductase: A cause and a potential target for the treatment of diabetic complications. Archives of Pharmacal Research, 44, 655-667.

[2] Balestri, F., Moschini, R., Mura, U., Cappiello, M., Del, Corso. A. 2022. In search of differential inhibitors of aldose reductase. Biomolecules, 12(4), 485.

[3] Papezikova, I., Pekarová, M., Chatzopoulou, M., Nicolaou, I., Demopoulos, V., Kubala, L., Lojek, A. 2008. The effect of aldose reductase inhibition by JMC-2004 on hyperglycemia-inducedendothelial dysfunction. Neuroendocrinology Letters, 29(5), 775.

[4] Kumar, P. A., Reddy, G. B. 2007. Focus on molecules: aldose reductase. Experimental eye research, 85(6), 739-740.

[5] Marchese, A. D., Larin, E. M., Mirabi, B., Lautens, M. 2020. Metal-catalyzed approaches toward the oxindole core. Accounts of Chemical Research, 53(8), 1605-1619.

[6] Zhou, F., Liu, Y. L., Zhou, J. 2010. Catalytic asymmetric synthesis of oxindoles bearing a tetrasubstituted stereocenter at the C-3 position. Advanced Synthesis & Catalysis, 352(9), 1381-1407.

[7] Pavlovska, T. L., Redkin, R. G., Lipson, V. V., Atamanuk, D. V. 2016. Molecular diversity of spirooxindoles, Synthesis and biological activity. Molecular diversity, 20, 299-344.

[8] Christy, N. A., Franks, A. S., Cross, L. B. 2005. Spironolactone for hirsutism in polycystic ovary syndrome. Annals of Pharmacotherapy, 39(9), 1517-1521.

[9] Kolancilar, H. 2019. DFT Yöntemi Kullanılarak 1, 3-Bis-{(2-Aminobenzoil) Amino} Propanın Teorik Hesaplamaları ve Bu Değerlerin Literatürdeki Deneysel Değerler ile Karşılaştırılması. Düzce Üniversitesi Bilim ve Teknoloji Dergisi, 7(3), 1319-1334.

[10] Chen, Y.H., Chao, S. D. 2018. Solving many-body Schrödinger equations with kinetic energy partition method. Annals of Physics, 388, 54-68.

[11] Güleç, Ö., Türkeş, C., Arslan, M., Demir, Y., Dincer, B., Ece, A., Küfrevioğlu, Ö. İ., and Beydemir, Ş. 2024. Novel spiroindoline derivatives targeting aldose reductase against diabetic complications: Bioactivity, cytotoxicity, and molecular modeling studies. Bioorganic Chemistry, 107221.

[12] Frisch, M. 2019. Gaussian09. http://www.gaussian.com (Erişim Tarihi: 05.04.2024).

[13] Madhavi Sastry, G., Adzhigirey, M., Day, T., Annabhimoju, R., Sherman, W. 2013. Protein and ligand preparation: parameters, protocols, and influence on virtual screening enrichments. Journal of Computer-Aided Molecular Design, 27(3), 221-234.

[14] Burley, S. K., Berman, H. M., Bhikadiya, C., Bi, C., Chen, L., Di, Costanzo. L., Christie, C., Dalenberg, K., Duarte, J. M., Dutta, S. 2019. RCSB Protein Data Bank: biological macromolecular structures enabling research and education in fundamental biology, biomedicine, biotechnology and energy. Nucleic acids research, 47(D1), 464-474.

[15] BIOVIA Discovery Studio D. SYSTÈMES BIOVIA Corporate Europe, BIOVIA 334 Cambridge Science Park Cambridge. 2016 http://accelrys.com/products/collaborativescience/biovia-discovery-studio/(Erişim Tarihi: 05.04.2024).

[16] Daina, A., Michielin, O., Zoete, V. 2017. SwissADME: a free web tool to evaluate pharmacokinetics, drug-likeness and medicinal chemistry friendliness of small molecules. Scientific reports, 7(1), 42717.

[17] Gören, K., Bağlan, M., Çakmak, İ. 2022. Theoretical Investigation of ^{1}H and ^{13}C NMR Spectra of Diethanol Amine Dithiocarbamate RAFT Agent. Journal of the Institute of Science and Technology, 12(3), 1677-1689.

[18] Altürk, S., Avcı, D., Tamer, Ö., Atalay, Y. 2017. Comparison of different hybrid DFT methods on structural, spectroscopic, electronic and NLO parameters for a potential NLO material. Computational and Theoretical Chemistry, 1100, 34-45.

[19] Bağlan, M., Gören, K., Yıldıko, Ü. 2023. HOMO–LUMO, NBO, NLO, MEP analysis and molecular docking using DFT calculations in DFPA molecule. International Journal of Chemistry and Technology, 7(1), 38-47.

[20] Wang, X., Yao, J. 2017. Improvement of the self-consistent-charge density-functional-tight-binding theory by a modified Mulliken charge. Theoretical Chemistry Accounts, 136(10), 124.

[21] Bağlan, M., Yıldıko, Ü., Gören, K. 2023. DFT Calculatıons and Molecular Dockıng Study ın 6-(2”-Pyrrolıdınone-5”-Yl)-Epıcatechın Molecule from Flavonoıds. Eskişehir Teknik Üniversitesi Bilim ve Teknoloji Dergisi B-Teorik Bilimler, 11(1), 43-55.

[22] Choudhary, V., Bhatt, A., Dash, D., Sharma, N. 2019. DFT calculations on molecular structures, HOMO–LUMO study, reactivity descriptors and spectral analyses of newly synthesized diorganotin (IV) 2-chloridophenylacetohydroxamate complexes. Journal of computational chemistry, 40(27), 2354-2363.

[23] Bağlan, M., Yıldıko, Ü., Gören, K. 2022. Computational Investigation of 5.5,7-trihydroxy-3,7-dimethoxy-4-4-O-biflavone from Flavonoids Using DFT Calculations and Molecular Docking. Adıyaman University Journal of Science, 12(2), 283-298.

[24] Bayoumy, A. M., Ibrahim, M., Omar, A. 2020. Mapping molecular electrostatic potential (MESP) for fulleropyrrolidine and its derivatives. Optical and Quantum Electronics, 52, 1-13.

[25] Bağlan, M., Gören, K., Yıldıko, Ü. 2023. DFT Computations and Molecular Docking Studies of 3-(6-(3-aminophenyl) thiazolo [1, 2, 4] triazol-2-yl)-2H-chromen-2-one (ATTC) Molecule. Hittite Journal of Science and Engineering, 10(1), 11-19.

[26] Shokr, E. K., Kamel, M. S., Abdel-Ghany, H., Ali, M., Abdou, A. 2022. Synthesis, characterization, and DFT study of linear and non-linear optical properties of some novel thieno [2, 3-b] thiophene azo dye derivatives. Materials Chemistry and Physics, 290, 46-66.

[27] Sakr, M. A., Sherbiny, F. F., El-Etrawy, A-A. S. 2022. Hydrazone-based materials; DFT, TD-DFT, NBO analysis, fukui function, MESP analysis, and solar cell applications. Journal of Fluorescence, 32(5), 1857-1871.

[28] Kurt, M., Babu, P. C., Sundaraganesan, N., Cinar, M., Karabacak, M. 2011. Molecular structure, vibrational, UV and NBO analysis of 4-chloro-7-nitrobenzofurazan by DFT calculations. Spectrochimica Acta Part A: Molecular and Biomolecular Spectroscopy, 79(5), 1162-1170.

[29] Mıhçıokur, Ö., Özpozan, T. 2017. Molecular structure, vibrational spectroscopic analysis (IR&Raman), HOMO-LUMO and NBO analysis of anti-cancer drug sunitinib using DFT method. Journal of Molecular Structure, 1149, 27-41.

[30] Khodja, I. A., Boulebd, H., Bensouici, C., Belfaitah, A. 2020. Design, synthesis, biological evaluation, molecular docking, DFT calculations and in silico ADME analysis of (benz) imidazole-hydrazone derivatives as promising antioxidant, antifungal, and anti-acetylcholinesterase agents. Journal of Molecular Structure, 1218, (12-27).

[31] Badran, A-S., Ibrahim, M. A. 2023. Synthesis, spectral characterization, DFT and in silico ADME studies of the novel pyrido [1, 2-a] benzimidazoles and pyrazolo [3, 4-b] pyridines. Journal of Molecular Structure, 1274, 13-54.

[32] Singh, S. P., Singh, N. I., Nongalleima, K., Doley, P., Singh, C. B., Sahoo, D. 2018. Molecular docking, MD simulation, DFT and ADME-toxicity study on analogs of zerumbone against IKK-β enzyme as anti-cancer agents. Network Modeling Analysis in Health Informatics and Bioinformatics, 7(1-8).